perturbation upon the H_a-Cl bond.

Reactions in the Matrix. HCN undergoes two association reactions with HF in the matrix due to the two ways HCN can bond to HF. Even though complex I has not been observed in the gas phase, the relative intensities for ν_s in complex II and the HF reagent absorption compared to ν_3^c in complex I and ν_3 of the HCN reagent suggest that complex I is the primary product formed upon codeposition of HF and HCN at 12 K. This occurs even though I is a weaker complex than $(HCN)_2$, based on the shift in ν_3, and the calculated hydrogen bond energy in complex I is nearly half that of complex II.[11] This implies that the formation of I must take place on the cold surface as the matrix is being formed, where the complex is frozen and trapped before rearrangement can take place. When the matrix is warmed above 20 K and recooled, most of product I disappears while the concentration of II in the matrix more than doubles. In general, an increase in the concentration of complexes similar to II is expected after diffusion is allowed in the matrix due to migration of unreacted HF to sites where unreacted base molecules are located, and this mechanism is probably responsible for some of the increase in the amount of II. This mechanism does not explain the decrease of I in the matrix or the extraordinarily large increase of II; however, the higher temperature (22 K) may allow a simple rearrangement of the HF submolecule to form the more stable complex II that is hindered at the lower temperature (12 K) and more rigid trapping sites in the matrix. The bent geometry of the complex means that the HF hydrogen could be attracted to the nitrogen while in a librational state with a large amplitude. The amplitude for the librations should be large because of the weak F-H bond and the low mass of the hydrogen. The Boltzmann factor, assuming a $\nu_{1\leftarrow 0}$ librational transition energy of 100 cm^{-1}, is on the order of 6×10^{-6} at 12 K, as opposed to a factor of about 1×10^{-3} at 22 K. The factor of 170 increase in the population of the $v = 1$ state that occurs on warming would increase the probability of the rearrangement so that over a period of time the amount of I would decrease. In the case of I formed with DF, where the initial yield was low and the amount increased upon warming, the amplitude of the libration is lower because of the increased mass, but the Boltzmann factor is near 2×10^{-4} at 12 K vs. 8×10^{-3} at 22 K because of the deuterium frequency shift. The higher Boltzmann factor suggests that even at 12 K there is enough population of the $v = 1$ state to account for a decrease in total yield over a long period of time, whereas the smaller difference in the factors between 12 and 22 K, along with the decreased amplitude of the libration motion, could result in an increase in the yield from the diffusion of DF to unreacted HCN. This mechanism would explain the concentration changes observed upon annealing, and also why very little of the HCl analogue of I was observed since the HCl experiments were all performed at 20 K.

Species III is formed when another HF attaches to complex II. In II the HF bond has been weakened by partial charge transfer, giving the fluorine atom more fluoride ion character. This near fluoride ion will have a high proton affinity and should be the site where the second HF molecule will attack. In the case where another HF molecule reacts with I, enough energy should be released by the reaction to allow rearrangement to III to take place.

Conclusions

The reaction between HF and HCN in the matrix has revealed interesting chemistry due to the dual acid-base nature of the hydrogen cyanide molecule. The matrix isolation technique has been particularly useful in that it allowed the observation of the less stable HF--HCN (I) complex, which has not been observed in the gas phase due to the ease of rearrangement to the more stable HCN--HF (II) structure. The HF--HCN complex was found to be nonlinear, as evidenced by splitting of the ν_2^c mode at 761 and 758 cm^{-1}, and to have a weaker association than $(HCN)_2$ as indicated by the smaller shift of ν_3^c (3271 cm^{-1}) for I as opposed to $(HCN)_2$. A mechanism for the rearrangement of I to II has been postulated to explain the changes that occur after annealing the matrix. The HCN--HF complex is linear, with the HF hydrogen bound to the nitrogen lone pair, as indicated by a single sharp HF librational mode. This contrasts with the "T-shaped" C_2H_2--HF complex involving HF hydrogen bonded to the C≡C π-orbital system. As in the case of several other HF complexes, complex II is attacked by a second HF at the fluorine, when unreacted HF is diffused through the matrix, resulting in a 2:1 HF complex with further perturbations in the vibrational modes.

Acknowledgment. The authors gratefully acknowledge financial support for this research from National Science Foundation Grant CH-79-10966.

Registry No. HF, 7664-39-3; HCN, 74-90-8; HCl, 7647-01-0.

Dynamics of Fatty Acids in Phospholipid Vesicles Using Spin Relaxation of Proton-Coupled Carbon-13 Spectra[1]

M. M. Fuson[†] and J. H. Prestegard*

Contribution from the Chemistry Department, Yale University, New Haven, Connecticut 06511.
Received April 26, 1982

Abstract: Spin relaxation of a ^{13}C-enriched methylene at the 2 position of myristic acid dissolved in small unilamellar vesicles has been examined under proton-coupled conditions. The data obtained are analyzed using a formalism that considers both autocorrelation and cross-correlation dipolar spectral densities leading to an improved definition of motional properties of a fatty acid chain in a membrane environment. Several motional models are tested for consistency with the data. Among suitable models, one that includes axial diffusion, rotational bond isomerization, and rapid wobbling of the director axis proves most appealing. This model assigns a short correlation time to bond isomerization, 4×10^{-11} s, and a rather long correlation time to axial diffusion, 2×10^{-7} s. A small C-H order parameter of −0.1 is predicted. This can be compared to order parameters obtained on multilayer membranes. The results are discussed in terms of implications for the effect of vesicle curvature and presence of membrane protein on acyl chain motion.

Introduction

It is widely recognized that biological membranes are dynamic structures which must allow both the movement of membrane proteins and the passage of metabolically important solutes. The dependencies of these membrane processes on both membrane lipid

[†] Department of Chemistry, University of Utah, Salt Lake City, UT 84112.

(1) Quinn, P. J. *Prog. Biophys. Molec. Biol.* **1981**, *38*, 1-104.

0002-7863/83/1505-0168$01.50/0

composition and the thermotropic phases of the lipid components have stimulated interest in the motional properties of constituent lipids themselves.[1] As a consequence, considerable effort has gone into characterizing the motion of lipid acyl chains in bilayer membrane systems, principally through nuclear magnetic resonance (NMR) studies.[2] These studies, utilizing ^1H, ^2H, and ^{13}C nuclei, typically provide information on *time scales* of motion (from spin relaxation) or on the extent of *averaging* of static interactions (expressed as order parameters). In analyzing this kind of information, investigators have employed numerous models for phospholipid motion.[3-9] In cases where direct comparison is possible, the studies agree in the time scales of two motions (10^{-7} to 10^{-8} s and 10^{-10} to 10^{-11} s). They differ, however, in the precise nature of molecular motions to which various correlation times are assigned.

The difficulty lies in the fact that models for motion can be tested for consistency with data but cannot be derived directly. With a limited range of data available, it is not surprising that a number of models prove to be consistent with observation. The purpose of this paper is to extend the range of data available by using the techniques of coupled spin relaxation developed by Grant,[10] the Volds,[11] and their co-workers to study the dynamics of a membrane probe, 2-^{13}C-3,3,4,4-tetra-^{2}H-myristic acid, (2-^{13}C-MA) dissolved in sonicated dimyristoylphosphatidylcholine (DMPC) vesicles. Previous studies have shown free fatty acids to intercalate into the lipid matrix in a nonperturbing manner. Characterization of the relaxation of the coupled $^{13}CH_2$ spin system in terms of both autocorrelation and cross-correlation spectral densities for dipolar interactions provides far greater detail on the dynamics of this methylene than previous methods. Our immediate goal will be to *discriminate* among possible models for acyl chain motion on as detailed and physically realistic a level as possible.

^{13}C relaxation studies are most frequently analyzed in terms of autocorrelation functions alone. The reason the addition of cross-correlation functions adds additional definition to the description of molecular motion of a methylene group can be qualitatively understood by closer examination of the origin of these functions. An autocorrelation spectral density, $J_{ijij}{}^{mn}(\omega)$, arising from a dipolar interaction between nuclei i and j, involves the Fourier transform of a time autocorrelation function, $\langle Y_2{}^m(\Omega_{ij};0)Y_2{}^n(\Omega_{ij};t)\rangle$, which relates the orientation of a dipolar vector at a given time relative to what it was at some earlier time. Thus, it effectively characterizes the reorientation of that vector. In a model describing diffusion of a general elipse, reorientation is related to the three diagonal elements of a diffusion tensor. To evaluate these elements, we would need to measure relaxation contributions from three linearly independent dipolar vectors. In a methylene group, dipolar autocorrelation functions exist for the two C–H vectors and the H–H vector, but these are all coplanar and thus do not reflect linearly independent contributions from the three elements of the diffusion tensor.

A cross-correlation spectral density involves the Fourier transform of a cross-correlation function, $\langle Y_2{}^m(\Omega_{ij};0)Y_2{}^n(\Omega_{kl};t)\rangle$, where the orientation of a vector, kl, at a given time is related to the orientation of a second vector, ij at an earlier time. In a three-spin system, these two vectors must have one end in common. To relate one of the vectors to the other, a rotation must occur about an axis perpendicular to the plane defined by the two dipolar vectors. The cross-correlation function in part describes the reorientation of this *rotation vector* and thus provides a spectral density related to a third noncoplanar vector in the ^{13}C methylene system.

The utility of coupled spin relaxation analysis has been illustrated through analysis of diffusion tensors for a number of small molecules containing isolated 3-spin systems, such as a ^{13}C methylene group.[12,13] Recently, we have shown in a study of malonic acid in solution, that by observing only the ^{13}C nucleus, using nonselective pulse techniques, and irrespective of remote spin populations, the diffusion tensor of the molecule could be completely characterized.[14] We will show that similar improved definition can be obtained for systems which require models having internal motions. Given the ubiquity of the methylene group and the ability to selectively enrich ^{13}C, this means it is possible to study a whole new class of problems involving segmental motion. The analysis of motion executed by a fatty acyl chain is but the first of these problems.

Theory

The theoretical description of the coupled spin relaxation of a ^{13}C methylene group (AX_2 spin system) as treated by density matrix techniques and Redfield–Bloch theory has been investigated in detail elsewhere.[10,14] The description leads to the treatment of spin–lattice relaxation of the AX_2 spin system in terms of "magnetization modes", ν, that are linear combinations of intensities for the component lines of the ^{13}C methylene multiplet. Observation of the time evolution of the magnetization modes leads to straightforward experimental evaluation of a series of dipolar spectral densities. The relationship of the magnetization modes to the more usual spectral densities is given for convenience in the Appendix.

The magnitudes of the spectral densities depend on the motion of the spin system. The connection between these experimental observables and time constants for various motions depends on an ability to calculate spectral densities from specific dynamical models. In doing this, we shall rely on formalisms developed by Szabo and collaborators.[3,15] Our results differ only in the inclusion of cross-correlation as well as autocorrelation spectral densities. We will outline results for the models most commonly proposed to explain acyl chain motions. These include models with isotropic plus axial diffusion, two or more axial diffusions, restricted diffusion, rotational isomeric states, and wobble of the chain director axis.

The dynamics of molecules in a sufficiently small vesicle system can be treated by regarding the vesicle as a spherical "macromolecule" with individual fatty acids having internal degrees of freedom. We begin by noting that given the symmetry of the probe molecule and the vesicle, and given the slow rate at which the fatty acid "flip-flops" from one side of the bilayer to the other, we can approximate the major internal motion of fatty acid in the bilayer as an axial rotation. For a diffusive axial rotation in a spherical macromolecule, we can write the following expression for the spectral density.

$$J_{ijkl}(\omega) = \xi_{ij}\xi_{kl}\frac{1}{4\pi}\sum_{m=-2}^{2}\frac{6D_i + m^2D_1}{(6D_i + m^2D_1)^2 + \omega^2}Y_2{}^m(\Omega_{ij})Y_2{}^m(\Omega_{kl}) \quad (1)$$

The notation is as follows. The $Y_2{}^m$ are second rank spherical harmonics, where the polar angles of the ij vector relative to the internal axis system are Ω_{ij}. ξ_{ij} is the dipolar interaction constant, defined as $\xi_{ij} = (6\pi/5)^{1/2}\gamma_i\gamma_j r_{ij}{}^{-3}$. γ_i and γ_j are the gyromagnetic ratios of nuclei i and j; r_{ij} is the internuclear distance. The superscripts have been dropped from the J because all J^{mn} can be expressed in terms of J^{00}.[16] D_i is the isotropic diffusion constant

(2) Jacobs, R. E.; Oldfield, E. *Prog. NMR Spectrosc.* **1981**, *14*, 113–136.
(3) Brainard, J. R.; Szabo, A. *Biochemistry* **1981**, *20*, 4618–4628.
(4) Petersen, N.; Chan, S. I. *Biochemistry* **1977**, *16*, 2657–2667.
(5) Gent, M. P. N.; Prestegard, J. H. *J. Magn. Reson.* **1977**, *25*, 243–262.
(6) Brown, M. F.; Seelig, J.; Haeberlen, U. *J. Chem. Phys.* **1979**, *70*, 5045–5053.
(7) London, R. E.; Avitabile, J. *J. Am. Chem. Soc.* **1977**, *99*, 7765–7776.
(8) Van der Leeuw, Y. C. W.; Stulen, G. *J. Magn. Reson.* **1981**, *42*, 434–445.
(9) Lee, A. G.; Birdsall, N. J. M.; Metcalfe, J. C.; Warren, G. B.; Roberts, G. C. K. *Proc. R. Soc. London, Ser. B* **1976**, *193*, 253–274.
(10) Werbelow, L. G.; Grant, D. M. *Adv. Magn. Reson.* **1977**, *9*, 189–299.
(11) Vold, R. L.; Vold, R. R. *Prog. NMR Spectrosc.* **1978**, *12*, 79–133.
(12) Mayne, C. L.; Grant, D. M.; Alderman, D. W. *J. Chem. Phys.* **1976**, *65*, 1648–1695.
(13) Kratchowill, A.; Vold, R. L.; Vold, R. R. *J. Chem. Phys.* **1979**, *71*, 1319–1324.
(14) Fuson, M. M.; Prestegard, J. H. *J. Chem. Phys.* **1982**, *76*, 1539–1545.
(15) Wittebort, R. J.; Szabo, A. *J. Chem. Phys.* **1978**, *69*, 1722–1736.

of the vesicle as a whole; D_1 is the axial diffusion constant. It is important to notice that the spectral density is a function of the orientation of the dipolar vectors relative to the internal rotation axis (Ω_{ij}, Ω_{kl}). Rotation about the average chain symmetry axis has $\theta_{ij} = \theta_{kl} = 90°$.

Equation 1 describes diffusive rotations about any rotation axis equally well. Only the polar coordinates (Ω_{ij}, Ω_{lk}) need to be adjusted. Introduction of additional diffusive rotations is straightforward. We can write for two diffusive rotations

$$J_{ijkl}(\omega) = \xi_{ij}\xi_{kl}\frac{1}{4\pi}\sum_{m,n}\frac{6D_i + m^2D_1 + n^2D_2}{(6D_i + m^2D_1 + n^2D_2) + \omega^2} \times d_{mn}^{(2)}(\beta_{12})^2 Y_2^n(\Omega_{ij}) Y_2^n(\Omega_{kl}) \quad (2)$$

where $d_{mn}^{(2)}(\beta_{12})$ is the reduced Wigner rotation matrix element and β_{12} is the angle between the two rotation axes. These might, for example, be a rotation about the acyl chain axis and a rotation about a C–C bond. The polar angles, Ω, are always relative to the last rotation axis, in our example the C–C bond. D_2 is the diffusion constant for motion about the second rotation axis and θ_{ij}, $\theta_{kl} = 70.5°$. Three internal rotations can be treated in an entirely analogous manner.

Rotations about fixed axes can be unnecessarily restrictive in the sense that we normally allow only a limited number of rotations. One way to generalize the model is the following. Instead of restricting off axis motions to being additional diffusive rotations along fixed axes, we can characterize them with an order parameter, S, describing the angular averaging that results when the axis about which the axial rotation takes place (the "director" axis) wobbles in a cone. This could be used to model, for instance, fluctuations of the entire acyl chain in the bilayer. The time correlation function necessary to describe this has been discussed by Brainard and Szabo.[3] The resulting spectral density expression is

$$J_{ijkl}(\omega) = \xi_{ij}\xi_{kl}\frac{1}{4\pi}\sum_{m}\left\{\left[S^2\frac{6D_i + m^2D_1}{(6D_i + m^2D_1)^2 + \omega^2}\right] + \left[(1 - S^2)\frac{6D_i + m^2D_1 + \frac{6 - m^2}{1 - S^2}D_w}{(6D_i + m^2D_1 + ((6 - m^2)/(1 - S^2))D_w)^2 + \omega^2}\right]\right\} \times Y_2^m(\Omega_{ij}) Y_2^m(\Omega_{kl}) \quad (3)$$

D_w is the diffusion constant of the wobble, a restricted diffusive rotation. The restricted rotation is characterized by an order parameter, S, defined as

$$S = \langle P_2(\cos\theta)\rangle = \frac{\int_0^\pi P_{eq}(\theta)P_2(\cos\theta)\sin\theta\, d\theta}{\int_0^\pi P_{eq}(\theta)\sin\theta\, d\theta} \quad (4)$$

where $P_{eq}(\theta)$ is the equilibrium orientational distribution. If this distribution is assumed to be uniform over some cone of semiangle, θ, $S = {}^1/_2\cos\theta(1 + \cos\theta)$.

In building a "rotational isomeric state" model, the methylene chain is regarded as existing in well-defined trans and gauche states, and dynamic processes occur through rapid jumps between these states.[17] This type of model has received considerable theoretical and experimental validation, epitomized in the molecular dynamics calculations on small hydrocarbons and polypeptide side chains performed recently by Levy and collaborators.[18]

(16) Hubbard, P. S. *Phys. Rev.* **1969**, *180*, 319–326.
(17) Flory, R. J. "Statistical Mechanics of Chain Molecules"; Interscience: New York, 1969.
(18) Levy, R. M.; Karplus, M.; Wolynes, P. G. *J. Am. Chem. Soc.* **1981**, *103*, 5998–6011.

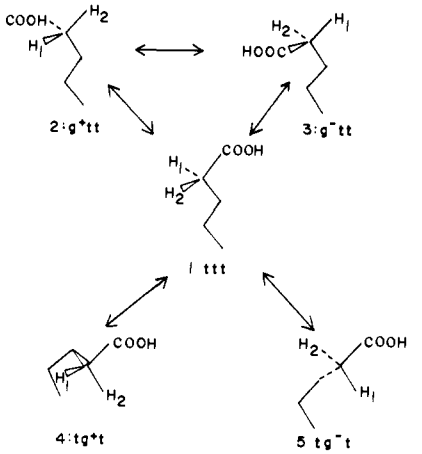

Figure 1. Conformations of the fatty acid chain used in jump models. Rotational isomers are given for the C_2–C_3, C_3–C_4, and C_4–C_5 bonds in that order. Numbers by each structure indicate positions in the columns and rows of the rate matrix in Table I.

Table I. Rate Matrices for 5-Site Jump Model

R =	−1.8132	0.4533	0.4533	0.4533	0.4533
	1	−2	1	0	0
	1	1	−2	0	0
	1	0	0	−1	0
	1	0	0	0	−1
$\hat{R}$ =	−1.8132	0.6733	0.6733	0.6733	0.6733
	0.6733	−2	1	0	0
	0.6733	1	−2	0	0
	0.6733	0	0	−1	0
	0.6733	0	0	0	−1
$\hat{X}$ =	0.5962	0	0	−0.8028	0
	0.4014	−0.3976	−0.3032	−0.2981	−0.7071
	0.4014	−0.3976	−0.3032	0.2981	0.7071
	0.4014	0.8264	−0.2591	0.2981	0
	0.4014	−0.0312	0.8655	0.2981	0
λ =	0	1	1	2.8133	3

A general equation for the spectral densities based on a master equation formalism for the rotational isomeric model can be written as

$$J_{ijkl}(\omega) = \xi_{ij}\xi_{kl}\frac{1}{4\pi}\sum_{m,n,l,k=1}^{p}\hat{X}_l^{(0)}\hat{X}_k^{(0)}\hat{X}_l^{(n)}\hat{X}_k^{(n)} + \frac{6D_i + m^2D_1 + \lambda_n}{(6D_i + m^2D_1 + \lambda_n)^2 + \omega^2} Y_2^m(\omega_{ij}) Y_2^m(\Omega_{kl}) \quad (5)$$

where p is the number of conformations. $\hat{X}^{(n)}$ and λ_n are the eigenvectors and eigenvalues of the symmetrized rate matrix, $\hat{R}$.[15]

We present here a specific jump model. It allows jumps about the C_2–C_3 and C_3–C_4 bonds. Only those conformations which keep C_1 level with or above C_2 in the bilayer are allowed. We assume that reorientation about the C_1–C_2 bond is rapid and able to maintain the hydrophilic interactions at the bilayer surface as long as the carboxylic acid moiety is not buried. Jumps are allowed about only one bond at a time. Populations of various conformers, P_i, are weighted to allow for the differing energies of gauche and trans states, assumed to be 0.5 kcal/mol. For computational simplicity only a single rate variable is used. Since three types of transition are possible, three rate constants, k_i, are in general required; two are related by

$$P_ik_i = P_jk_j \quad (6)$$

This yields one variable for all gauche–trans type transitions, but it leaves undefined gauche–gauche jump rates. We arbitrarily assign them the same value as gauche to trans rates (that is, the rate of leaving gauche states is the same without regard for the destination conformation).

As defined, this jump model allows all conformations with a single gauche bond about either bond C_2–C_3 or C_3–C_4 as well as

the all-trans conformer. These five conformations are detailed in Figure 1. Note that jumps between conformations 2 and 4 are not allowed because this requires isomerization of two bonds. Jumps between 4 and 5 are not allowed because this would swing the head group down into the bilayer. R, $\hat{R}$, $\hat{X}$, and λ are given in Table I for this model. More restricted jump models can be generated by setting additional elements of the rate matrix to zero.

The main shortcoming of jump models is widely recognized to be that they do not take into account the nonideal nature of conformational jumps in real molecules. We expect that torsional oscillations about C–C bonds on a picosecond time scale will result in the spin system sampling more of space than is implied by jumps between ideal geometries. This viewpoint is again validated by comparison of molecular dynamics results and simple dynamic models of the type we have been discussing.[18] To compensate for the absence of vibrational averaging, we shall extend the formalism of Brainard and Szabo discussed above by combining eq 3 and 5. D_w will be fixed to the picosecond time scale to mimic the effects of vibrational averaging and S will approximate the amplitude of these motions.

Experimental Section

Isotopically labeled materials were obtained as follows: 2-^{13}C-acetic acid (90 atom % ^{13}C), $^2H_2SO_4$ (96 atom % ^{2}H), and $LiAl^2H_4$ (99 atom % ^{2}H) were obtained from MSD Isotopes, Merck and Co. (Rahway, NJ). ^2H_2O (99.75 atom % ^{2}H) was obtained from J. T. Baker Chemical Co. (Phillipsburg, NJ). DMPC was obtained from Sigma Chemical Co. (St. Louis, MO) and used without further purification. All other chemicals were reagent grade from standard suppliers.

Fatty acids were deuterated at the α position by heating with $^2H_2SO_4$ at 120 °C for 24 h. 2-^{13}C-MA was synthesized from 2,2-di-^{2}H-lauric acid by reduction with $LiAl^2H_4$, bromination with PBr_3, and the addition of 2-^{13}C-acetic acid according to the method of Pfeffer et al.[19]

NMR Sample Preparation. A mixture consisting of 13.8 mg (58 μM) MA and 0.4 g (0.58 mM) DMPC was dissolved in $CHCl_3$ and then dried under vacuum for ~6 h. The lipid mixture was then suspended in 8 mL of ^2H_2O buffer (0.1 M PO_4^{2-}, 0.02% NaN_3, 0.5 mM EDTA) by vortexing and the p^{2}H was adjusted to 7.4 with NaO^2H. This suspension was sonicated for 6 h at 50 °C in a Branson Model E bath sonicator to produce vesicles. Two samples were made in this way. They were identical except that in one the myristic acid was isotopically labeled. The resulting vesicle solutions were placed in 20-mm flat-bottomed NMR tubes and maintained at temperatures above 30 °C. The multilayer sample for ^{2}H NMR was prepared analogously using 2,2-di-^{2}H-MA; 0.5 g of the lipid mixture was suspended in 0.5 g ^1H_2O buffer and heated to 50 °C for 6 h with frequent vortexing.

NMR Experiments. NMR relaxation experiments were performed on a Bruker CXP-200 as outlined previously.[14] With the exception of experiments for measurement of ν_4, these are based on simple inversion recovery sequences. ν_4 experiments require a pair of measurements, one of which includes a ^{1}H 90° pulse just before acquisition. Initial conditions were established with both ^{13}C inversion and ^{1}H inversion. Temperatures were 45 ± 1 °C; 8k data points were collected over a sweep width of 4000 Hz with a recycle delay 3 s, and 1850 transients were collected at each of nine τ values. Difference spectra between labeled and nonlabeled samples and between ν_4 pairs were obtained using commercial software in which a multiplicative constant was adjusted to achieve the best baseline in the lipid methylene region. Peak intensities were measured using a software integration routine.

^{2}H spectra were acquired using the quadrupole echo pulse sequence.[20] The sweep width was 100 000 Hz, τ values were 60 and 50 μs, respectively, and the recycle delay was 0.1 s.

Photon Correlation Spectroscopy.[21] Vesicle size distributions were characterized using photon correlation spectroscopy. The sample was prepared from the sample used for NMR spectroscopy, described above. This vesicle solution was diluted 100:1 with an identical buffer solution which had been filtered through a 0.4-μm Millipore filter. The solution was then centrifuged at 30 000 g for 20 min to remove dust and large lipid aggregates. The resulting supernatant was carefully removed and placed in a 10-mm cylindrical cell.

Quasielastic light scattering measurements were made using an argon ion laser, λ = 488 nm, and an autocorrelation function calculated by a Malvern K7025 4-bit correlator interfaced to an LSI-11 computer. The correlator was set up with 112 data channels and 16 baseline channels separated from the data channels by a delay equivalent to another 112 channels. To assure minimal correlator overflows, laser light levels were reduced with crossed polarizers. Only data where experimental baselines were within a standard deviation of the theoretical baseline were used. The temperature was 44.1 °C and the scattering angle was 90°.

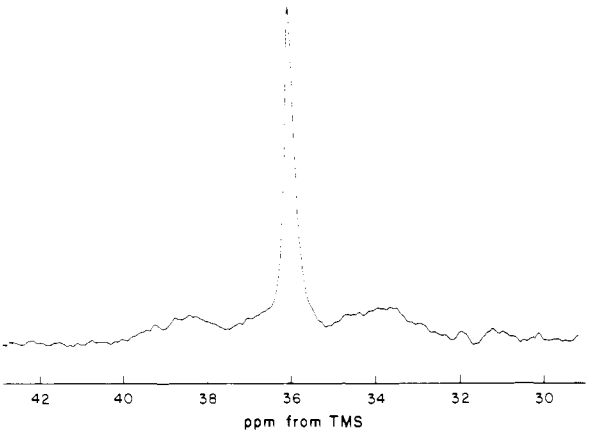

Figure 2. The 50.3-MHz ^{13}C difference spectrum of sonicated DMPC vesicles containing unenriched and 90% enriched 2-^{13}C-MA; 7200 transients requiring 6 h were collected for each spectrum.

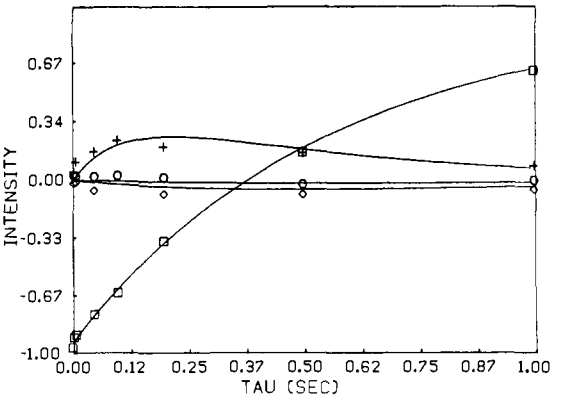

Figure 3. Data from coupled spin-relaxation experiments. Vertical scale is normalized so that the equilibrium ^{13}C intensity is 1; (□), (◇), and (○): ν_1, ν_3, and ν_4 following ^{13}C inversion; (+), ν_4 following ^{1}H inversion. Solid lines are the calculated fit of the rotational isomerization plus torsion model described in the text.

Results

Since the ^{13}C resonance of the fatty acid C_2 falls just downfield of intense background resonances from the lipid acyl chain methylenes, difference spectra removing the background resonances were necessary to accurately measure intensities of the proton coupled C_2 multiplet. An example of the resulting spectra is shown in Figure 2. As discussed by Prestegard and Grant, the broadened outer lines of the multiplet are indicative of rapid axial motion with the axis near the normal to the methylene plane.[22]

NMR longitudinal relaxation measurements characterize the time evolution of four magnetization modes. These are: (1) ν_1 (the total ^{13}C magnetization) after ^{13}C inversion; (2) ν_3 (the difference in ^{13}C outer and inner multiplet line intensities) after ^{13}C inversion; (3) ν_4 (the difference in outer line and inner line triplet component intensities) after ^{13}C inversion; and (4) ν_4 after ^{1}H inversion. These data are plotted in Figure 3. The variance per point, estimated from the root-mean square signal to noise and experimental reproducibility, is ±0.05 relative to an equilibrium ^{13}C intensity defined to be 1.

In addition to longitudinal modes, spin–spin relaxation times may be obtained from the widths of the individual lines. For the outer lines T_2 is 5.3 ms (R_2 = 190 s^{-1}). For the inner line the

(19) Pfeffer, P. E.; Silbert, L. S. *J. Org. Chem.* **1972**, *37*, 451–458.
(20) Davis, J. H.; Jeffrey, K. R.; Bloom, M.; Valic, M. I.; Higgs, T. P. *Chem. Phys. Lett.* **1976**, *42*, 390–394.
(21) Bargeron, C. B. *J. Chem. Phys.* **1974**, *61*, 2134–2138.
(22) Prestegard, J. H.; Grant, D. M. *J. Am. Chem. Soc.* **1978**, *100*, 4664–4668.

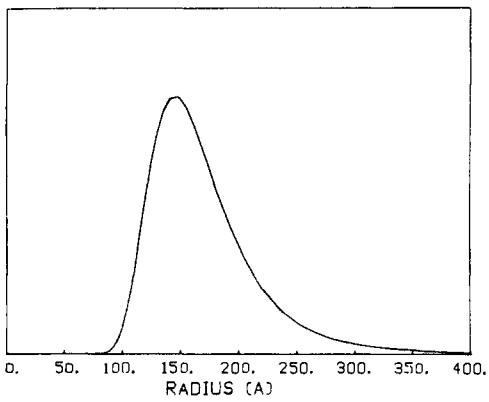

Figure 4. Distribution of vesicle sizes calculated from photon correlation spectroscopy. Vertical scale is arbitrary, but proportional to the number of scatterers of a given size.

apparent T_2 is 40 ms (R_2 = 25 s^{-1}). In the limit of slow isotropic motion and fast axial rotation the inner line is a single Lorentzian,[22] but we cannot be sure we are truly in this limit. If we are not, the line shape is more complicated and cannot be analyzed in terms of a single time constant. In the following data analysis, therefore, we will use only the outer line R_2.

Data analysis is performed using a multivariable direct search fitting routine as described previously.[14] Variables fit are the carbon inversion intensity, two random field spectral densities, and dynamical parameters appropriate for each motional model. Fixed input parameters include the proton inversion intensity, the vesicle tumbling diffusion constant, and the dipolar interaction geometries (to be discussed below). Proton inversion intensities are measured independently observing the effects of J modulation on the ^{13}C multiplet. Departures from theoretical modulation amplitudes indicate a proton inversion efficiency of 0.90 ± 0.03.

The vesicle size distribution and hence a vesicle tumbling diffusion constant is characterized by photon correlation spectroscopy (as described by Koppel and Bargeron[23]). The autocorrelation spectrum is fit with a cumulant expansion truncating the fit after 3 cumulants.[21] The cumulants are defined as

$$K_1 = \langle q^2 D \rangle$$

$$K_2 = \langle (q^2 D - \langle q^2 D \rangle)^2 \rangle$$

$$K_3 = \langle (q^2 D - \langle q^2 D \rangle)^3 \rangle$$

where q is the scattering vector, $q = (4\pi n/\lambda) \sin \theta/2$, and n is the refractive index. The three cumulants are, respectively, related to the mean of the distribution of diffusion constants, its breadth, and its asymmetry. We find

$$K_1 = 1.17 \pm 0.05 \times 10^4$$

$$K_2 = 2.55 \pm 1.06 \times 10^7$$

$$K_3 = 2.31 \pm 9.28 \times 10^{10}$$

A comparison of K_3 to $(K_1)^3$ (1.6×10^{12}) provides a rough estimate of the degree of asymmetry of the distribution. This ratio as measured here is very small. Combined with the lack of significance of the value of K_3, this suggests it is reasonable to assume that K_3 is zero and to model the distribution of diffusion constants as Gaussian. After adjusting for the scattering intensity dependence on particle size and for the fact that our particles are hollow shells,[24] we can generate a size distribution as shown in Figure 4. This distribution has a maximum at a radius of 146 ± 25 Å in good agreement with previous measurements using electron microscopy. The diffusion constant for vesicle tumbling calculated from this most probable radius is 9.4×10^4 s^{-1}.

The angles defining the geometry of the dipolar interactions relative to the axes of motion are important parameters of the relaxation behavior. Here we will assume perfect tetrahedral geometry for the acyl chain. This is not exactly correct, but it is very close and should not introduce important errors. Our starting point is the all-trans chain. Relative to the long axis of the molecule the C–H vector will have polar angles of θ = 90° and, relative to each other, the C–H vectors will have an angle of $\Delta\phi$ = 109.5°. A C–C bond axis has an angle of 35.25° relative to the long-chain axis. C–C bond axes relative to each other are 109.5°. The C–H vectors relative to the C–C bond axis have θ = 70.5° and $\Delta\phi$ = 120°.

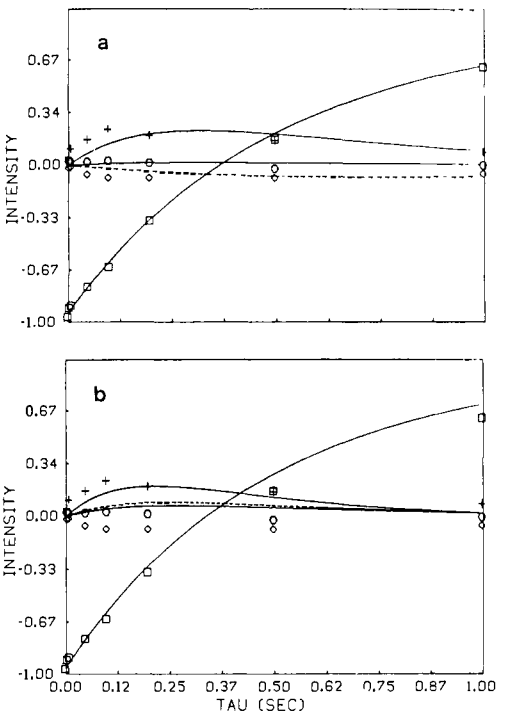

Figure 5. Best fit of a model which includes an isotropic component and a rotation about an axis. The symbols for the data are (□), (◇), and (○): ν_1, ν_3, and ν_4 following ^{13}C inversion; (+) ν_4 following ^1H inversion. The lines represent the calculated fit. The dashed line is ν_3 after ^{13}C inversion. In (a) the axis is a C–C bond, ($\Delta\phi$ = 120°). In (b) the axis is the bilayer normal ($\Delta\phi$ = 109°).

Except for ^{13}C inversion intensity, the remainder of our variables are motional in character and values are optimized during data fitting with results shown in Table II for each motional model considered. Motional parameters are expressed as correlation times (τ_c) rather than diffusion constants because of the greater ease of comparison of diffusive and jump motions: for diffusive motions τ_k is equal to $1/6D_k$ while for jumps the correlation time is the inverse of the jump rate.

Two measures of "goodness of fit" are given. The R_2 of the outer line predicted by the fit is listed. This should be compared to a measured value of 190 s^{-1}. Also listed is the χ^2 for the fit of the longitudinal modes. An optimal fit will have a χ^2 of 1. Fitted values of the ^{13}C inversion intensity are not listed. Typical values are 0.93 ± 0.03. For fits with χ^2 values near 1 such as the rotational isomeric-wobble model, theoretical recovery curves produce good visual fits to the data as shown in Figure 3. It is immediately apparent from Table II that an isotropic model gives a bad fit of the data even though the correlation time is an adjustable parameter.

Columns 2 and 3 of Table II are models where the fatty acid molecule is allowed to undergo two motions with fitted time scales: one isotropic and the other a diffusive axial rotation. Column 2 shows the result for a model where the axial rotation is assumed to be the rotation of the entire acyl chain in the bilayer. Then the H–C–H angle is 109.5°. While the fit is considerably improved over a purely isotropic model of motion, χ^2 is not minimized. Column 3 is the result of fitting an entirely analogous model, but with the axial rotation occurring about a C–C bond. Then the H–C–H angle is 120°. χ^2 is significantly reduced compared to column 2. These differences are visually illustrated

(23) Koppel, D. E. *J. Chem. Phys.* **1972**, *57*, 4814–4820.
(24) Goll, J. H.; Stock, G. B. *Biophys. J.* **1977**, *9*, 26–273.

Table II. Parameters Obtained by Fitting Data to Various Models

model	1 isotropic	2 isotropic + axial ($\Delta\phi = 109.5°$)	3 isotropic + axial ($\Delta\phi = 120°$)	4 vesicle tumbling + axial ($\Delta\phi = 120°$)	5 1 bond rotation	6 2 bond rotations	7 restricted diffusion	8 5-site jump	9 5-site jump + wobble
τ_i	$3.7 \pm 0.1 \times 10^{-8}$	$4.3 \pm 0.1 \times 10^{-8}$	$9.4 \pm 0.3 \times 10^{-8}$	$[1.8 \times 10^{-6}]$	$[1.8 \times 10^{-6}]$	$[1.8 \times 10^{-6}]$	$[1.8 \times 10^{-6}]$	$[1.8 \times 10^{-6}]$	$[1.8 \times 10^{-6}]$
τ_1		$2.3 \pm 0.2 \times 10^{-11}$	$1.4 \pm 0.1 \times 10^{-11}$	$1.0 \pm 0.1 \times 10^{-11}$	$4.8 \pm 2.0 \times 10^{-12}$	$1.3 \pm 0.1 \times 10^{-7}$	$2.4 \pm 1.4 \times 10^{-11}$	$4.3 \pm 0.7 \times 10^{-10}$	$1.6 \pm 0.3 \times 10^{-7}$
τ_2, τ_J					$4.5 \pm 0.1 \times 10^{-11}$	$2.4 \pm 2.0 \times 10^{-11}$		$9.2 \pm 0.9 \times 10^{-12}$	$3.7 \pm 0.3 \times 10^{-11}$
τ_3, τ_W						$2.3; 1.0 \times 10^{-11}$	$6.3; 4.0 \times 10^{-11}$		$[10^{-12}]$
S (single mode)							0.230 ± 0.003		0.563 ± 0.007
j_C	0.0	0.0	0.0	0.0	0.0	0.0	0.0	0.0	0.0
j_H	0.09 ± 0.03	0.71 ± 0.16	0.42 ± 0.08	0.44 ± 0.08	0.44 ± 0.14	0.66 ± 0.15	0.67 ± 0.14	0.71 ± 0.14	0.62 ± 0.14
longitudinal χ^2	26.56	5.07	1.84	7.74	2.37	1.32	1.30	1.49	1.19
calcd R_2	224.0	197.0	190.0	3561.0	871.0	190.0	190.0	572.0	190.0

in Figure 5. Figure 5a shows the modes generated by the fit given in column 3. It only deviates significantly from the data in the early time portion of ν_4 after ^1H inversion. The modes generated from column 2 are similar *except* for ν_3 after ^{13}C inversion. The ν_3 time course shown in Figure 5b deviates from zero in the positive rather than negative direction. Thus we can see, even on this simple level, that we have the ability to discriminate between motions which differ only in orientation of a rotation axis.

The above models allow isotropic motions on any time scale. While in one case we have come close to reproducing the data, the fitted value of the isotropic motion, 9×10^{-8} s, is not susceptible to straightforward interpretation. The one isotropic motion we do know about and have characterized is the overall tumbling of the vesicle. This has a correlation time of 1.8×10^{-6} s. We shall now propose models where this isotropic correlation time is set and the relaxation behavior is fit by varying only parameters for the motion of the fatty acid within the bilayer. If we do this, and return to the model of a single diffusive rotation about a C–C bond, we get the result shown in column 4 of Table II. The predicted outer line R_2 is now extremely large. Longitudinal modes are not fit well either. Clearly we must investigate models with additional off-axis motions.

Two of these models are given in columns 5 and 6 of Table II. These models allow a sequence of diffusive rotations. Column 5 shows the results when rotations are allowed about the acyl chain axis and one C–C bond. Column 6 is the same except that a second C–C bond rotation is also allowed. For one bond rotation it can be readily seen that while the longitudinal relaxation is approaching a decent fit, the zero frequency spectral densities which dominate R_2 are still badly reproduced. Introduction of another bond rotation (column 6) results in a nearly optimal fit.

A second way to introduce off-axis motions is to allow the spin system to undergo fluctuations in a cone about the rotation axis. The result of fitting such a model to data is shown in column 7. Here the molecule is modeled as undergoing rotation about a C–C bond axis and in addition wobbling in a cone about that axis. The fit is quite good. The amplitude of this wobbling motion is characterized by the order parameter, S. If we use the simple model of motion with a cone of constant probability with semiangle θ, we can calculate $\theta = 70°$ for the fitted value of $S = 0.23$.

Although this level of description fits the relaxation data, it is far more likely that motion corresponds to isomerizations about carbon–carbon bonds rather than diffusive rotations. We therefore have examined a number of jump models for acyl chain isomerization in the bilayer. These models start with vesicle tumbling and a freely fit rotation about the acyl chain axis and then allow jumps among a variety of chain conformations. Although we examined models involving as many as nine conformations, no significant improvement in the fits was achieved beyond the five-site model described earlier. The fit using this model is reported in column 8. The longitudinal modes are fit quite well, but the outer line width is much too broad. This is not surprising as jump models do not efficiently sample all of the configurational space. We expect this to be reflected most dramatically in the line width.

More realistic sampling of space can be achieved by introducing motions on a picosecond time scale that can mimic torsional oscillations about individual bonds. Motions on this time scale will not contribute to the frequency dependence of the spectral densities but will instead result in a reduced dipolar interaction. Because torsional oscillations can result from motions about many C–C bonds, it is not trivial to model them analytically. Arbitrarily, we model them as resulting in the spin system being with equal probability anywhere in a cone of semiangle θ. The fit achieved using such a model is listed in column 9 of Table II. It is the best we have achieved and is that shown in Figure 3. The fitted value of S is consistent with $\theta = 47°$.

Since all the above models introduce partial rapid averaging of dipolar interactions that can be characterized by an order parameter, S, it would be nice to have a direct measurement of this quantity. This can be provided by ^2H NMR. Unfortunately, only measurements on multilayers are straightforward. Therefore,

we examined the ^2H order parameter in a multilayer system containing 2,2-di-^2H-MA. The observed splitting is 24.3 kHz. Using the accepted value of the quadrupole coupling constant for paraffinic chains, 170 kHz, we calculate the ^2H order parameter, S_{CD}, to be −0.19. This is in good agreement with the measurements of Stockton et al. using selectively deuterated stearic acid in egg yolk lecithin.[25] Its comparison to values used in fitting fatty acid data will be left to the Discussion.

Discussion

We have presented arguments in our Introduction that the inclusion of spin-relaxation experiments which allow specific evaluation of cross-correlation spectral densities should improve our ability to discriminate between various proposed models for phospholipid motion. The analysis presented in Table II and in Figure 5 suggests that this is true. Notice that with the exception of the simple isotropic model all models optimize with one correlation time within an order of magnitude of 10^{-11} s, and most optimize with a second correlation time within an order of magnitude of 10^{-7} s. This is consistent with previous studies on lipid vesicle systems which do not use cross-correlation data.[3-9] This fact suggests that at least the short time scales of motions can be determined from conventional spin-relaxation experiments without dramatic dependence on choice of motional model.

Determination of appropriate molecular descriptions for the geometry of motions is more difficult. In this context it is important to reiterate that we cannot prove a specific model but we can test various models for consistency with data. We can also draw attention to common features of models producing good fits of experimental data.

Seen with this perspective, the data presented here allow the following general conclusions with regard to models. First, a model of simple isotropic motion can again be dismissed. This is apparent from the multiplet line shapes (drastically broadened outer lines while the inner line remains sharp are characteristic of rapid axial motion in the limit of slow isotropic motions). It is also apparent from the departure of all of the longitudinal modes, as characterized by a large χ^2. Second, even with such a simple mode as an isotropic motion plus an axial rotation, we can begin to distinguish between models which differ in the geometry of the motion. In fitting the data, we have present two different "isotropic plus axial" models. In one the axial rotation is about the long chain axis, while in the other it is about a C–C bond axis. As shown in Figure 5 and columns 2 and 3 of Table II, we can clearly distinguish between these. Modeling the motion as a rotation about a C–C bond in addition to isotropic motions does reproduce all of the general trends of the data, even though the fit is not completely optimized. Rather than conclude that C–C bond rotation is correct, we believe this indicates that fast axial motion about the bilayer normal alone is not sufficient and that one must consider rapid off-axis motions such as those which can arise from bond isomerizations.

The most general model that allows rapid off axis motion is a restricted rotation in a cone of constant probability. Using this model for motions other than vesicle tumbling and rotation about a C–C bond, we obtain a completely optimized fit as described in Table II, column 7. This model is very similar to models used by Peterson and Chan[4] and by Gent and Prestegard[5] and, thus, is appropriate for comparison to their work. Our data are fit by an axial C–C bond rotation correlation time of $\tau_c = 2.4 \times 10^{-11}$ s and a correlation time for restricted rotation in a cone of semiangle 70° of 6.3×10^{-11} s.

The magnitude of the correlation time for the restricted rotation and the angular excursion are very similar to those found by Gent and Prestegard.[5] In the previous work, restricted diffusion on an annulus of ±60 was taken as a crude description of the motion caused by coupled β-gauche isomerizations. The correlation time (analogous to fixing both our correlation times to the same value) of 5×10^{-11} s is in good agreement with the value found here. We can calculate S_{CD} predicted by our model to be −0.08. This is in apparent agreement with the prediction of Chan and collaborators based on a model of similar construction. However, contrary to their model we do not see evidence for off-axis motions in the range of 10^{-7} to 10^{-9} s. When we attempt to fit the data while requiring the correlation time for the restricted rotation to be of order 10^{-8} s, χ^2 for the fit of the longitudinal modes never decreases below 12 (an order of magnitude larger than optimum). Again, this suggests that rapid, large amplitude off-axis motions are necessary.

The models summarized in columns 6 through 9 of Table II are more closely linked to molecular structure, and it is interesting to examine the molecular motions with which time constants of various magnitudes become associated. Columns 6 and 9 present models in which additional off-axis motions are allowed. Both fit data very well. They also introduce slower motions with time scales on the order predicted by previous models in the literature. It is interesting that the slow motion is associated with a rotation about the average chain axis and not an off-axis motion. It is perhaps significant that recent studies have questioned the existence of off-axis slow motions.

Van der Leeuw and Stulen, for example, have recently looked at the proton relaxation of lipid membranes oriented at the magic angle.[8] They conclude that T_2's are not affected by motions on a time scale greater than 10^{-10} s. Wolber and Hudson, using fluorescence lifetimes and time-resolved polarization anisotropy measurements, conclude that no motions causing large chain reorientations relative to the bilayer normal are taking place in the range of 10^{-5} to 10^{-8} s.[26]

Of the models which produce good fits of the data, the most intuitively appealing is the rotational isomeric model with director wobble (column 9). This model is also the only model that correctly predicts the width of the inner line of the ^{13}C multiplet (8 Hz). This piece of data was not part of the original data fitted. Here, too, it is useful to examine time constants and order parameters for various motions with respect to physical expectations. In addition to vesicle tumbling, the rotational isomeric model incorporates three kinds of motion. First, there is an axial rotation about the chain axis on a time scale of 1.6×10^{-7} s. Second, there is isomerization about the C_2–C_3 and C_3–C_4 bonds to give single gauche isomers with a correlation time of 3.7×10^{-11} s. Finally, torsional oscillations on a picosecond time scale cause the spin system to sweep out a cone of semiangle 47°.

The time scale for axial diffusion seems extremely slow if we view this as characteristic of an all-trans chain rotating as a rod in the bilayer. If we consider a more irregular molecule, the time scale proves a little more reasonable. We can calculate the correlation time under stick boundary conditions ($\tau_c = V\eta/kT$) if we can estimate the volume of MA (V) and the bilayer viscosity (η). Modeling MA as a cylinder, the cross-sectional area of the cylinder we will assume to be one-half of the cross-sectional area of DMPC (70 Å^2). We estimate the length of the cylinder as 21 Å. Estimates of the viscosity of bilayers are in the range of 1 to 100 cP.[9,27,28] We shall use 50 cP. Then $\tau_c \simeq 10^{-8}$ s. While this differs from our observed value by an order of magnitude, we would expect to err on the short side. Real acyl chains are not cylinders and will be at least somewhat entangled with neighboring chains.

The 4×10^{-11} s time scale for rotational isomerizations agrees with time scales of motions assigned to bond isomerizations by a number of authors.[4-9] Time scales of 10^{-10} s are also appropriate for isomerizations in simple hydrocarbons.[28]

Aside from these rapid jumps, we have wobble on a picosecond time scale over a range of 47°. The picosecond time scale is not critical since it is too fast to contribute to relaxation. The 47° range seems plausible when considering that we are attempting to model torsional bond oscillations, and the angular range of the

(25) Stockton, G. W.; Polnaszek, C. F.; Tulloch, A. P.; Hasan, F.; Smith, I. C. P. *Biochemistry* **1976**, *15*, 954–966.

(26) Wolber, P. K.; Hudson, B. S. *Biochemistry* **1981**, *20*, 2800–2810.

(27) Seelig, J.; Seelig, A. *Q. Rev. Biophys.* **1980**, *13*, 19–61.

(28) Levy, R. M.; Karplus, M.; McCannon, J. A. *Chem. Phys. Lett.* **1979**, *65*, 4–11.

torsional oscillation about a single C–C bond, whether estimated by using a very simple model of the torsional motion as a harmonic oscillator or by carrying out a full-blown molecular dynamics calculation, is estimated to be ±20° to 30°.[28] Since our averaging must represent the cumulative effect of torsions in several bonds, it seems reasonable to allow an angular variation of ±47°.

While our primary purpose has been to test various models for acyl chain motion with an extended set of spin-relaxation data, it is appropriate to use our most probable model to comment briefly on implications for current problems in membrane biophysics.

One controversy still open in the literature is the effect of bilayer curvature on lipid order and dynamics. Many studies, including this one, have used small, unilamellar vesicles as model bilayer systems. The question of what effect the high radius of curvature might have on the structural and dynamic processes is important in extrapolating results to more extended bilayer systems. Chan and collaborators have suggested that this effect is fairly large, leading, for instance, to a change in the ^2H order parameter of a factor of 2 to 3 and in the time scale of the slow motion from 10^{-7} to (10^{-8} to 10^{-9}) s.[29] Bloom and his collaborators[30] and Brown[6] suggest the opposite, that little effect exists. Our data indicate significant structural dependence. As noted above, for the multilayer system $S_{CD} = -0.19$. We can calculate, considering all internal motions that would average the quadrupolar interaction, an S_{CD} for the unilamellar vesicles of –0.1. This change is in reasonable agreement with Chan's prediction of a reduction of the order parameter by a factor of 2 to 3. Given our model for motion, this reduction stems largely from bond isomerizations. In other words, in the vesicle system there are more gauche conformers. This kind of change in the number of gauche conformers has been predicted recently by Dill and Flory in statistical mechanical studies of bilayer structures.[31] Using a lattice model to treat the chain packing, they predict that relative to the flat bilayer, in a small unilamellar vesicle the number of gauche bonds will increase by a factor of 2 in the outer monolayer while decreasing slightly in the inner monolayer. Given that $^2/_3$ of the molecules are in the outer monolayer, this would lead to a change in S_{CD} from –0.19 to –0.13, not far from what we observe. There are also some Raman spectroscopic data which qualitatively indicate changes in the proportion of gauche bonds upon sonication.[32] One, of course, cannot ignore the fact that the strong correlation between multilayer order parameters and ^2H line widths in vesicles observed by Stockton et al. supports the opposite point of view.[25]

One of the main goals of studying lipid dynamics is to be able to explain the properties of biological membranes. One subject on which understanding of lipid dynamics may shed light is the effect of perturbations to the bilayer system introduced by incorporating cholesterol or intrinsic membrane proteins. Over the past several years, quite a few systems have been studied by spin relaxation techniques with the consistent result that the perturbations introduced are small.[33-37] This is especially true for T_1, but T_2 perturbations are also generally small. To some extent our current model does provide insight into these observations. Little wagging of long segments of the chain takes place in our model. Instead, the motion dominating T_2 is a complex jittering about a number of closely connected bonds coupled with an axial diffusion. Introducing a spatial boundary will cause only minimal perturbations of such short-range and symmetric motions. The motion of chains in contact with an irregular protein surface may be very similar to those described here.

In the above analysis, one must keep in mind that our results are based on observation of a fatty acid probe rather than of a phospholipid molecule itself. The fatty acid was chosen in the interest of minimizing synthetic effort and to provide a system a little more amenable to analysis on the basis of simple motional models. Nevertheless, there are data to indicate that fatty acid probes provide a reasonable representation of phospholipid acyl chain motions. For example, in pure fatty acid bilayer phases the deuterium order parameter measured for material labeled at the 2 position is –0.3.[38] Phospholipids labeled near the ester linkage typically show order parameters of –0.2.[39] In the present study the measured deuterium order parameter is –0.19, showing that the properties of the fatty acid in a phospholipid bilayer more closely resemble those of the lipid matrix. Despite this support for the validity of fatty acid probes, experiments described here can be and are being extended to observations on phospholipids themselves.

Acknowledgment. This work was supported by grants from the National Science Foundation, PCM 7821101, and from the National Institutes of Health, GM 19035.

Appendix

The relaxation of weakly coupled spin systems in terms of magnetization modes has been treated in detail in a series of papers by Werbelow, Grant, and co-workers.[10] The magnetization modes used in the treatment can most simply be viewed as linear combinations of spin deviation density matrix elements, $\chi_{\alpha\alpha'}(t)$, where α and α' denote one of the spin states for the AX_2 spin system. We shall indicate state by number according to the following scheme. Here the + and – signs used in symmetrized product functions symbolize spin functions with magnetic quantum number $m = \pm^1/_2$, respectively. They are written in the order A, X, X.

$$|1\rangle = +++$$

$$|2\rangle = -++$$

$$|3\rangle = +\frac{1}{\sqrt{2}}(+-\quad+\quad-+)$$

$$|4\rangle = +\frac{1}{\sqrt{2}}(+-\quad-\quad-+)$$

$$|5\rangle = -\frac{1}{\sqrt{2}}(+-\quad-\quad-+)$$

$$|6\rangle = -\frac{1}{\sqrt{2}}(+-\quad+\quad-+)$$

$$|7\rangle = +--$$

$$|8\rangle = ---$$ (A1)

While some elements of $\chi_{\alpha\alpha'}$ may correspond directly to observables, for example χ_{12} to transverse magnetization of an outer line of the A multiplet, these are not always the most convenient set and the $\chi_{\alpha\alpha'}$ are recombined into magnetization modes which correspond more closely to independent observables. The particular set that we use to describe longitudinal magnetization are defined as

$$\nu_1 = \tfrac{1}{2}(\chi_{11} - \chi_{22} + \chi_{33} + \chi_{44} - \chi_{55} - \chi_{66} + \chi_{77} - \chi_{88})$$

$$\nu_2 = (\chi_{11} + \chi_{22} - \chi_{77} - \chi_{88})$$

$$\nu_3 = \tfrac{1}{2}(\chi_{11} - \chi_{22} - \chi_{33} - \chi_{44} + \chi_{55} + \chi_{66} + \chi_{77} - \chi_{88})$$

$$\nu_4 = (\chi_{11} - \chi_{22} - 2\chi_{33} + 2\chi_{66} + \chi_{77} - \chi_{88})$$ (A2)

(29) Bocian, D. F.; Chan, S. I. *Ann. Rev. Phys. Chem.* **1978**, *29*, 307–335.
(30) Bloom, M.; Burnell, E. E.; MacKay, A. L.; Nichol, C. P.; Valic, M. I.; Weeks, G. *Biochemistry* **1978**, *17*, 5750–5761.
(31) Dill, K. A.; Flory, P. J. *Proc. Natl. Acad. Sci. USA* **1981**, *78*, 676–680.
(32) Gaber, B. P.; Peticolas, W. L. *Biochim. Biophys. Acta* **1977**, *465*, 260–274.
(33) Stoffel, W. O.; Zierenberg, O.; Scheefers, H. *Hoppe-Seyler's Physiol. Chem.* **1977**, *358*, 865–871.
(34) Longmuir, K. J.; Capaldi, R. A.; Dalquist, F. W. *Biochemistry* **1977**, *16*, 5746–5751.
(35) Fleischer, S.; McIntyre, J. O.; Stoffel, W.; Tunggal, B. D. *Biochemistry* **1979**, *18*, 2420–2428.
(36) Ong, R. L.-D.; Prestegard, J. H. *Biophys. J.* **1982**, *37*, 80–82.
(37) Zumbulyadis, N.; O'Brien, D. F. *Biochemistry* **1979**, *18*, 5427–5432.
(38) Charvolin, J.; Manneville, P.; Deloche, B. *Chem. Phys. Lett.* **1973**, *23*, 345–348.
(39) Seelig, A.; Seelig, J. *Biochemistry* **1974**, *13*, 4839–4845.

From inspection of eq A2 and the definition of states, eq A1, it is clear that ν_1 corresponds to total A (^{13}C) magnetization, ν_2 to total X (^1H) magnetization, ν_3 to the difference in magnetization of outer and inner lines of the A (^{13}C) multiplet, and ν_4, the difference in magnetization of the outer lines and triplet component of the inner line of the A (^{13}C) multiplet.

The time evolution of spin deviation density matrix elements is most conveniently given in terms of the Redfield formalism,[40] which yields

$$\frac{d}{dt}\chi_{\alpha\alpha'}(t) = \sum_{\alpha''\alpha'''} R_{\alpha\alpha'\alpha''\alpha'''}\chi_{\alpha''\alpha'''}(t) \quad \text{(A3)}$$

For a case where only dipolar interactions are considered, elements of the relaxation matrix, R, can in turn be written in terms of the spherical harmonics, Y_2^μ, components of the spin tensor, T_2^μ, and the dipolar interaction constant, ξ_{ij}. Thus

$$R^{ijkl}{}_{\alpha\alpha'\alpha''\alpha'''} = \sum_{m,n}[2J^{mn}{}_{ijkl}(\omega_{\alpha\alpha''})\langle\alpha|T_2^m(ij)|\alpha''\rangle \times \langle\alpha'''|T_2^n(kl)|\alpha'\rangle - \delta_{\alpha\alpha''}\sum_\beta J^{mn}{}_{ijkl}(\omega_{\alpha'''\beta})\langle\alpha'''|T_2^m(ij)|\beta\rangle \times \langle\beta|T_2^n(kl)|\alpha'\rangle - \delta_{\alpha'\alpha'''}\sum_\beta J^{mn}{}_{ijkl}(\omega_{\alpha''\beta})\langle\alpha|T_2^m(ij)|\beta\rangle \times \langle\beta|T_2^n(kl)|\alpha''\rangle] \quad \text{(A4)}$$

where $\omega_{\alpha\alpha'}$ is the frequency of an α to α' transition. For an isotropic fluid the dipolar spectral densities, $J^{mn}{}_{ijkl}$, are given by

$$J^{mn}{}_{ijkl}(\omega) = (-1)^m\delta_{m-n}J^{00}{}_{ijkl}(\omega) = \xi_{ij}\xi_{kl}\int_0^\infty \langle Y_2^0(\Omega_{ij}(0))Y_2^0(\Omega_{kl}(t))\rangle \cos(\omega t)\, dt \quad \text{(A5)}$$

The spherical harmonics in these expressions are written in terms of polar angles, Ω, of internuclear vectors relative to the laboratory frame with the z axis the static field axis. They can be rewritten in terms of chemical bond or molecule fixed axes and analytical expressions for spectral densities can be derived from the time dependence of various dynamical models as described in the text.

We have made provision for contributions by relaxation mechanisms other than directly bonded dipolar interactions in the AX_2 group by treating these as random field interactions. This is a conventional choice in coupled spin relaxation experiments where there are no important intramolecular interactions other than those among A and X nuclei. We have used a simplified treatment in which random field spectral densities at A and X sites, j_A and j_X, are treated as variables in fitting data. Incorporation of these terms in relaxation expressions has been discussed previously.[14]

The time evolution of the magnetization modes follows easily from the time evolution of spin deviation density matrix elements discussed above since the magnetization modes are simple linear combinations of the χ's. Time evolution can be expressed as

$$-\frac{d}{dt}\nu_i = \sum_j A_{ij}\nu_j \quad \text{(A6)}$$

Before listing the elements of the evolution matrix A_{ij}, we will simplify notation for spectral densities, $J^{mn}{}_{ijkl}$, by expressing all J^{mn} in terms of J^{00}, dropping superscripts and by replacing nucleus subscripts, i, j, k, l, by A or X and not repeating the subscript where a single subscript or pair of subscripts occurs in succession. For example, the auto-correlation spectral density $J^{11}{}_{ijij}$ becomes J_{AX}. The elements of the evolution matrix are thus given as

$$\begin{aligned}
A_{11} &= 2J_{AX}(\omega_A) + 4J_{AX}(\omega_X + \omega_A) + \tfrac{2}{3}J_{AX}(\omega_X - \omega_A) + 2j_A\\
A_{12} &= 2J_{AX}(\omega_X + \omega_A) - \tfrac{1}{3}J_{AX}(\omega_X - \omega_A)\\
A_{13} &= 4J_{XAX}(\omega_X + \omega_A) + \tfrac{2}{3}J_{XAX}(\omega_X - \omega_A) + 2J_{XAX}(\omega_A)\\
A_{14} &= -2J_{XAX}(\omega_X + \omega_A) - \tfrac{1}{3}J_{XAX}(\omega_X - \omega_A)\\
A_{21} &= 4J_{AX}(\omega_X + \omega_A) - \tfrac{2}{3}J_{XAX}(\omega_X - \omega_A)\\
A_{22} &= J_{AX}(\omega_X) + 2J_{AX}(\omega_X + \omega_A) + \tfrac{1}{3}J_{AX}(\omega_X - \omega_A) + J_{XX}(\omega_X) + 4J_{XX}(2\omega_X) + 2j_X\\
A_{23} &= 4J_{XAX}(\omega_X + \omega_A) - \tfrac{2}{3}J_{XAX}(\omega_X - \omega_A)\\
A_{24} &= 2J_{AXX}(\omega_X) - 2J_{XAX}(\omega_X + \omega_A) + \tfrac{1}{3}J_{XAX}(\omega_X - \omega_A)\\
A_{31} &= 2J_{XAX}(\omega_A)\\
A_{32} &= 2J_{AXX}(\omega_X)\\
A_{33} &= 2J_{AX}(\omega_A) + 2J_{AX}(\omega_X) - 2J_{XAX}(\omega_X) + 2j_A + 4j_X - 4j_{XX}\\
A_{34} &= J_{XX}(\omega_X) + J_{XAX}(\omega_X) + 2j_X\\
A_{41} &= 4J_{XAX}(\omega_A) - 4J_{XAX}(\omega_X + \omega_A) - \tfrac{2}{3}J_{XAX}(\omega_X - \omega_A)\\
A_{42} &= 6J_{AXX}(\omega_X) - 2J_{XAX}(\omega_X + \omega_A) + \tfrac{1}{3}J_{XAX}(\omega_X - \omega_A)\\
A_{43} &= -\tfrac{8}{3}J_{AX}(0) + \tfrac{8}{3}J_{XAX}(0) + 4J_{AX}(\omega_A) + 2J_{AX}(\omega_X) - 2J_{XAX}(\omega_X) - 4J_{AX}(\omega_X + \omega_A) - \tfrac{2}{3}J_{AX}(\omega_X - \omega_A) + 4j_H - 4j_{XX}\\
A_{44} &= \tfrac{4}{3}J_{AX}(0) - \tfrac{4}{3}J_{XAX}(0) + J_{AX}(\omega_X) + 2J_{XAX}(\omega_X) + 2J_{XAX}(\omega_X + \omega_A) + \tfrac{1}{3}J_{AX}(\omega_X - \omega_A) + 3J_{XX}(\omega_X) + 2j_A + 2j_X + 4j_{XX}
\end{aligned} \quad \text{(A7)}$$

Note that recovery of the various modes depends in different ways on autocorrelation, cross-correlation, and random field spectral densities. For example, recovery of ν_3 after perturbation of ν_1 depends most directly on J_{XAX}, while after perturbation of ν_2 it depends on J_{AXX}. Multiparameter fitting of recovery curves can lead to evaluation of spectral density elements, or directly to specific variables in dynamic models.

Registry No. MA, 544-63-8; DMPC, 13699-48-4.

(40) Redfield, A. G. *Adv. Magn. Reson.* **1965**, *1*, 1–30.